Protein Science (1992), *1*, 1508–1521. Cambridge University Press. Printed in the USA.

Solution-state structure by NMR of zinc-substituted rubredoxin from the marine hyperthermophilic archaebacterium *Pyrococcus furiosus*

PAUL R. BLAKE,[1] JAE-BUM PARK,[2] ZHI HAO ZHOU,[2] DENNIS R. HARE,[3] MICHAEL W.W. ADAMS,[2] AND MICHAEL F. SUMMERS[1]

[1] Department of Chemistry and Biochemistry, University of Maryland Baltimore County, Baltimore, Maryland 21228
[2] Department of Biochemistry and Center for Metalloenzyme Studies, University of Georgia, Athens, Georgia 30602
[3] Hare Research, Inc., 18943 120th Avenue N.E., Bothell, Washington 98011

(RECEIVED April 29, 1992; REVISED MANUSCRIPT RECEIVED June 19, 1992)

Abstract

The three-dimensional solution-state structure is reported for the zinc-substituted form of rubredoxin (Rd) from the marine hyperthermophilic archaebacterium *Pyrococcus furiosus*, an organism that grows optimally at 100 °C. Structures were generated with DSPACE® by a hybrid distance geometry (DG)-based simulated annealing (SA) approach that employed 403 nuclear Overhauser effect (NOE)-derived interproton distance restraints, including 67 interresidue, 124 sequential ($i-j=1$), 75 medium-range ($i-j=2$–5), and 137 long-range ($i-j>5$) restraints. All lower interproton distance bounds were set at the sum of the van Der Waals radii (1.8 Å), and upper bounds of 2.7 Å, 3.3 Å, and 5.0 Å were employed to represent qualitatively observed strong, medium, and weak NOE cross peak intensities, respectively. Twenty-three backbone–backbone, six backbone–sulfur (Cys), two backbone–side chain, and two side chain–side chain hydrogen bond restraints were include for structure refinement, yielding a total of 436 nonbonded restraints, which averages to >16 restraints per residue. A total of 10 structures generated from random atom positions and 30 structures generated by molecular replacement using the backbone coordinates of *Clostridium pasteurianum* Rd converged to a common conformation, with the average penalty (= sum of the square of the distance bounds violations; ±standard deviation) of 0.024 ± 0.003 Å^2 and a maximum total penalty of 0.035 Å^2. Superposition of the backbone atoms (C, Cα, N) of residues A1–L51 for all 40 structures afforded an average pairwise root mean square (rms) deviation value (±SD) of 0.42 ± 0.07 Å. Superposition of all heavy atoms for residues A1–L51, including those of structurally undefined external side chains, afforded an average pairwise rms deviation of 0.72 ± 0.08 Å. Qualitative comparison of back-calculated and experimental two-dimensional NOESY spectra indicate that the DG/SA structures are consistent with the experimental spectra. The global folding of *P. furiosus* Zn(Rd) is remarkably similar to the folding observed by X-ray crystallography for native Rd from the mesophilic organism *C. pasteurianum*, with the average rms deviation value for backbone atoms of residues A1–L51 of *P. furiosus* Zn(Rd) superposed with respect to residues K2–V52 of *C. pasteurianum* Rd of 0.77 ± 0.06 Å. The conformations of aromatic residues that compose the hydrophobic cores of the two proteins are also similar. However, *P. furiosus* Rd contains several unique structural elements, including at least four additional hydrogen bonds and three potential electrostatic interactions. Four of these interactions involve the nonconservatively substituted Glu 14, Ala 1, and Trp 3 residues. The combined findings are consistent with the proposal that stabilization of the N-terminal residues inhibits the β-sheet from "unzipping" at elevated temperatures (Blake, P.R., Park, J.-B., Bryant, F.O., et al., 1991, *Biochemistry 30*, 10885–10895). In view of the high structural similarities between this hyperthermophilic protein and *C. pasteurianum* Rd, this effect may serve as the dominant mechanism by which *P. furiosus* Rd is stabilized at high temperatures.

Keywords: distance geometry; hyperthermophile; iron–sulfur protein; NMR; protein structure; rubredoxin; zinc substitution

Within the past decade, novel genera of bacteria that flourish at remarkable temperatures up to 110 °C have been isolated from marine hydrothermal vents (Fiala & Stetter, 1986; Stetter, 1986; Adams, 1990; Stetter et al., 1990). Termed hyperthermophiles, these organisms possess significant biotechnological potential due to their abilities to metabolize a variety of substrates, including elemental sulfur and carbohydrates, and to produce such gases as CO_2, H_2, and H_2S. In addition, they have the potential to provide hyperthermostable enzymes with biotechnological and industrial utility. Unfortunately, present knowledge of these organisms is limited mainly to papers

Reprint requests to: Michael F. Summers, Department of Chemistry and Biochemistry, University of Maryland Baltimore County, Baltimore, Maryland 21228.

describing their isolation, and very little is known about the novel biochemistry that enables these life forms to thrive under extreme temperature conditions. Except for our preliminary findings (Blake et al., 1991b, 1992b,c), molecular-level information regarding the factors that enable proteins from hyperthermophiles to remain folded and functional at temperatures at or exceeding 100 °C is primitive or lacking.

We have initiated NMR studies of rubredoxin (Rd) from the marine hyperthermophile *Pyrococcus furiosus* (an organism that grows optimally at 100 °C) in order to determine its structural and dynamic properties and to gain insights into the determinants of protein hyperthermostability. To overcome NMR relaxation problems associated with the paramagnetic iron in the native protein, studies have focused on the zinc- and cadmium-113-substituted forms of the protein, Zn(Rd) and ^{113}Cd(Rd). Two-dimensional (2D) ^{1}H NMR analyses enabled determination of the resonance assignments and secondary structure of Zn(Rd). The major findings were that the three-stranded antiparallel β-sheet is extended to include the N-terminal amino acid, and that the positively charged amino group of the N-terminal Ala 1 residue is positioned in close proximity to the side chain carboxyl of Glu 14 (Blake et al., 1991b). These interactions are not possible in rubredoxins from mesophiles. (The amino acid sequences of *P. furiosus* and *Clostridium pasteurianum* rubredoxins are given below. See Blake et al. [1991b] for a complete listing of known Rd amino acid sequences.) In addition, ^{1}H and ^{113}Cd NMR studies of ^{113}Cd(Rd) revealed that the NH–S hydrogen bonds formed by the amide protons of residues I7, C8, I40, and C41 contain significant covalent character (Blake et al., 1992b,c).

Pf: AKWVCLICGYIYDEDAGDPDNGISPGTKFEELPDDWVCPICGAPKSEFEKLED

Cp: MKKYTCTVCGYIYDPEDGDPDDGVNPGTDFKDIPDDWVCPLCGVGKDEFEEVEE

We have now extended the secondary structural studies of Zn(Rd), and have determined its three-dimensional (3D) solution-state structure via a hybrid distance geometry (DG)/simulated annealing (SA) approach. Two-dimensional nuclear Overhauser effect (NOESY) back-calculations were employed to evaluate the consistence between the calculated structures and the experimental NMR data. In combination with X-ray structural studies of the native protein (carried out independently from the present study; see companion paper [Day et al., 1992]), these studies provide the first 3D structure determination of a protein from a hyperthermophilic organism.

Results and discussion

NH proton exchange

Deuterium exchange experiments were carried out on Zn(Rd) as a probe for hydrogen bonding. Figure 1 shows the downfield region of the ^{1}H NMR spectra obtained for Zn(Rd) in 90% H_2O/10% D_2O (bottom) and upon dissolution of the lyophilized sample into D_2O. After incubation at 25 °C for 20 min, 28 distinguishable NH signals were observed, indicating that these protons are involved in hydrogen bonding and/or are sequestered from the solvent (Fig. 1). Backbone NH signals that were clearly absent after incubation for 20 min at 25 °C include those for the following residues: D13, E14, S24, K28, F29, E30, D34, S46, K50, E52, and D53. The following side chain protons were also clearly absent in this spectrum: N21-NH$^{\epsilon,z}$, Y12-OH, and T27-OH. The relative exchange rates of additional amide protons with resonances that overlapped with aromatic or other NH proton signals could not be determined. After incubation for 36 h at 25 °C, NH signals were still detectable for residues W3, V4, C5, I7, C8, Y10, Y12, W36, V37, C38, I40, C41, G42, and E49. During this 36-h time interval, a 2D NOESY (Jeneer et al., 1979; Macura & Ernst, 1980) spectrum was obtained, which enabled assignment of the above NH signals. After incubation at 25 °C for a total of 77 h, the sample temperature was raised in 20 °C increments (with equilibration for 30 min at each temperature) to a final temperature of 80 °C. The intensities of several NH signals remained essentially unaffected, even after subjecting the protein to these extreme temperatures (Fig. 1). The protons that appear to be least sensitive to exchange include the backbone NH protons of residues W3, V4, C5, Y10, Y12, W36, C38, I40, C41, A43, K45, and F48. Of the six NH protons proposed to form NH–S hydrogen bonds, the Y10 and A43 NH protons exhibit the slowest exchange with solvent deuterium. Interestingly, these protons did not give rise to detectable NH–S hydrogen bond-mediated scalar coupling to ^{113}Cd in ^{113}Cd(Rd), and exhibited weak coupling to Hg in ^{199}Hg(Rd) (Blake et al., 1992b,c).

NOE-derived distance restraints

Cross peak intensities in a 200-ms 2D NOESY spectrum were qualitatively assigned as strong, medium, or weak and were used to assign upper interproton distance restraints of 2.7 Å, 3.3 Å, and 5.0 Å, respectively (Gronenborn et al., 1991). An additional 0.5 Å was added to the upper bound for proton pairs involving methyl groups (Clore et al., 1987). To assist in the identification of spin diffusion cross peaks, an 80-ms 2D rotating frame Overhauser effect (ROESY) (Bothner-by et al., 1984) spectrum was collected for comparison with the NOESY spectrum. Peaks attributed to spin diffusion were not used to generate distance restraints. A total of 403 interproton distance restraints were derived from the NOESY data, including totals of 67 interresidue, 124 sequential, 75 medium range (2–5 residues), and 137 long-range (>5 residues) restraints. A total of 33 additional restraints were included for hydrogen bonds implicitly defined by NOESY

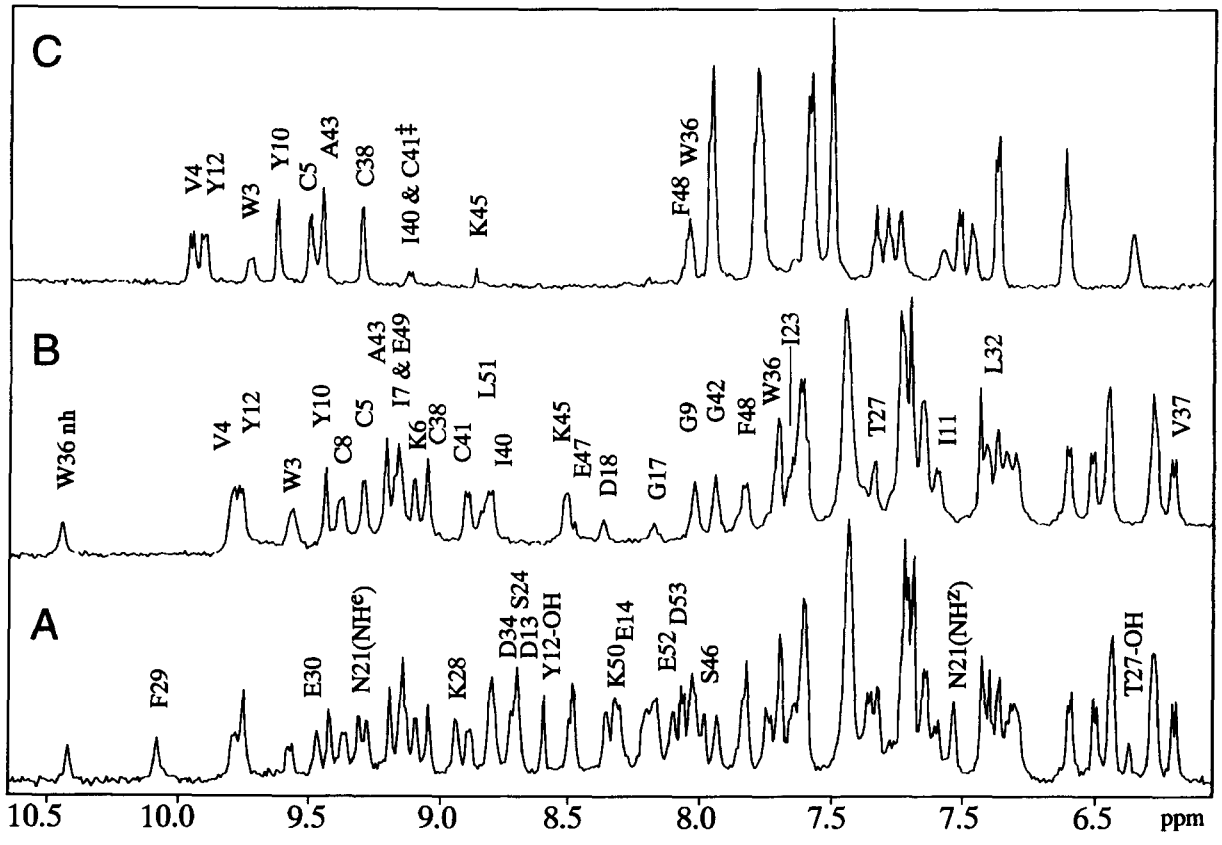

Fig. 1. Stacked plot showing the downfield region of ^{1}H NMR spectra obtained for *Pyrococcus furiosus* zinc-substituted rubredoxin (Zn(Rd)) in 90% H_2O/10% D_2O solution (**A**) (pH 6.2, 25 °C) and after dissolution of a lyophilized sample into D_2O, followed by incubation at 25 °C for 20 min (**B**). Distinguishable signals for protons that exchanged readily and that did not undergo rapid exchange with water protons are labeled in A and B, respectively. After incubation at 25 °C for 77 h, the sample temperature was raised in 20 °C increments (with equilibration for 30 min at each temperature) to a final temperature of 80 °C. The spectrum subsequently obtained at 80 °C (**C**) still exhibits signals for at least nine backbone NH protons (labeled). No detectable signal loss was observed for the Y10 and A43 NH protons that are apparently involved in Type-II NH-S hydrogen bonding. ‡Overlapping signals assigned from temperature-dependent chemical shift behavior.

cross peaks, hydrogen exchange rates, and/or characteristic chemical shifts (see below), giving an average of 16.3 nonbonded distance restraints per residue. An additional eight restraints were included to enforce 2.3-Å Zn-S distances and proper sp^3 sulfur hybridization. No restraints were included to control the zinc coordination geometry (i.e., S-Zn-S bond angles). Initial models were generated without regard to prochiral stereochemical assignments of geminal protons. Stereochemical assignments for 25 diastereotopic methylene proton pairs and for the stereochemically nonequivalent Leu 32 methyl groups were made subsequently on the basis of relative intraresidue and nearest-neighbor NOE cross peak intensities. A complete listing of the distance restraints is included in the supplementary materials on the Diskette Appendix.

Structure generation and refinement

A total of 40 initial DG/SA structures were generated on the basis of the NOE-derived distance restraints and the 18 hydrogen bond restraints that define the three-stranded antiparallel β-sheet, the NH-S tight turns of the metal-binding site, and a short anti-parallel β-sheet-like region adjacent to the metal-binding site (Tables 1, 2). Of these 40 structures, 30 were generated via a molecular replacement method (below) using the backbone coordinates (C, Cα, N, O, Cβ) of *C. pasteurianum* Rd as initial atom positions (obtained from the Brookhaven Protein Data Bank), and 10 were generated from randomized atom positions. Forty "final" structures were generated subsequently with 15 additional hydrogen bond restraints for the 3_{10}-helical corners, β-turns, and other hydrogen bonds identified from characteristic αH(i)-NH(i + 3) NOESY cross peak patterns, relative orientations of side chains in initial structures, reduced chemical exchange rates, and for the case of Asn 21, a characteristic downfield-shifted NH^{ε} proton signal. The general procedures used for structure generation and refinement are described below.

Molecular replacement refinement was achieved by implementation of an in-house program that converts the C,

Table 1. *Distance geometry restraints and structural statistics*[a]

Distance restraints	
Interresidue	67
Sequential	124
Medium range ($\|i-j\|$ = 2–5 residues)	75
Long range ($\|i-j\|$ > 5 residues)	137
Hydrogen bonds	33[b]
Metal-ligand	8
Mean restraints per residue	16.34[b]

	DG/SA structures[b,c]		Comparison with Cp Rd[d]	
Structural statistics	Initial	Final	Initial DG/SA	Final DG/SA
Mean total penalty	0.024 ± 0.002	0.024 ± 0.003		
Max/min total penalty	0.032/0.020	0.035/0.021		
Max individual violation	<0.03	<0.03		
Mean pairwise rms deviation				
Backbone atoms[e]				
Residues 5–10, 38–43	0.16 ± 0.06	0.16 ± 0.06	0.33 ± 0.02	0.33 ± 0.02
Residues 15–26	0.50 ± 0.14	0.35 ± 0.11	0.52 ± 0.09	0.52 ± 0.10
Residues 1–14, 27–51	0.39 ± 0.07	0.36 ± 0.07	0.69 ± 0.07	0.66 ± 0.07
Residues 1–51	0.57 ± 0.13	0.42 ± 0.07	0.93 ± 0.13	0.77 ± 0.06
All heavy atoms[f]				
Residues 1–51	0.88 ± 0.12	0.72 ± 0.08		
All residues	1.24 ± 0.23	1.08 ± 0.22		

[a] Penalty (= squared sum of the distance violations) and root mean square (rms) deviation values are in units of Å^2 and Å, respectively; distance violations are in units of Å. Values are reported as a mean ± SD.

[b] Initial structures were generated with only the 18 hydrogen bonds that define the three-stranded β-sheet and the NH–S tight turns, whereas final structures were generated with 33 hydrogen bond restraints. Each hydrogen bond restraint actually consists of two restraints, including XH–O/S and X–O/S (X = N, O) distances. The additional hydrogen bond restraints served only to ensure reasonable donor–acceptor distances and did not influence either the general orientation of the side chains or the backbone conformation.

[c] Results for 40 distance geometry/simulated annealing (DG/SA) structures, including 10 structures generated from random atom coordinates and 30 structures generated by a molecular replacement approach (see text).

[d] Comparison of the 40 *Pyrococcus furiosus* zinc-substituted rubredoxin DG/SA structures with appropriate residues in the X-ray structure of native *Clostridium pasteurianum* rubredoxin (Cp Rd) (Watenpaugh et al., 1979).

[e] Backbone atoms C, Cα, and N.

[f] All C, N, and O atoms.

Cα, N, O, and Cβ atom coordinates of Brookhaven Protein Data Bank (PDB) format files to coordinates readable by DSPACE. Coordinates for the remaining amide protons, α-protons, and side chain atoms were assigned values identical to those of the N, Cα, and Cβ atoms, respectively. By this approach, the PDB coordinates for *C. pasteurianum* Rd were used to generate a crude *P. furiosus* Rd template, and this initial structure was subjected to minimal SA and conjugate gradient minimization (CGM). The structure obtained exhibited a moderately high penalty value (ca. 4 Å^2) but contained many of the secondary structural elements established by previous NMR studies (Blake et al., 1991b). In particular, this initial structure contained crude elements of the three-stranded antiparallel β-sheet and the metal-binding site.

A total of 30 structures were generated from the above model by performing high-velocity SA (to a penalty of ca. 250–300 Å^2) followed by CGM. Due to ambiguities resulting from signal degeneracies in the ^{1}H NMR spectra, the initial structures were generated using only ca. 75% of the total number of distance restraints ultimately identified in the NOESY data. The NOE-derived distance restraints were initially treated with an approximately fourfold higher weighting function relative to bond length and angle restraints and an approximately eightfold higher weighting function relative to the van der Waals radius restraints. The relative weightings of the NOE-derived interproton and primary distance restraints were varied systematically during the CGM calculations until they ul-

Table 2. *Root mean square deviations relative to the mean coordinates of the final structures*[a]

Atoms and residues	⟨DG/SA⟩ – DG/SA	⟨DG/SA⟩ – Cp Rd
C, Cα, N of 5–10, 38–43	0.11 ± 0.03	0.31
C, Cα, N of 15–26	0.24 ± 0.09	0.46
C, Cα, N of 1–14, 27–51	0.25 ± 0.06	0.66
C, Cα, N of 1–51	0.29 ± 0.07	0.71
All heavy atoms of 1–51	0.50 ± 0.03	

[a] Mean coordinates (denoted by ⟨DG/SA⟩) calculated from the superposition of C, Cα, and N atoms of all 40 final DG/SA structures (residues A1–L51). DG/SA, distance geometry/simulated annealing; Cp Rd, native *Clostridium pasteurianum* rubredoxin.

timately achieved equal values. When additional CGM was unable to reduce the total penalty, the penalty value was compared to a predefined value to determine if the structure was to be saved as is or subjected to additional rounds of SA/CGM refinement.

An additional 10 structures were generated by performing 15-Å randomizations of all atoms, followed by application of SA/CGM refinement. The initial structures typically exhibited "tangled" backbone conformations that could not be readily untangled using standard 3D SA/CGM refinement techniques. High penalty barriers associated with these structures were successfully overcome by application of four-dimensional (4D) SA/CGM refinement that included initial SA to a target penalty of ca. 700 $Å^2$, followed by lower velocity CGM. Experimental restraints were initially assigned a 6-fold higher weighting function relative to bond length, bond angle, and atom radii restraints (see macro programs included in the supplementary materials on the Diskette Appendix) for simulated annealing and a 20-fold higher weighting for CGM refinement. Structures were subsequently subjected to additional 3D SA/CGM refinement as described above.

By inspection of first-generation structures, it was possible to assign cross peaks in the NOESY spectrum that could not be assigned initially due to spectral overlap and signal degeneracies. Distance restraints associated with these newly assigned cross peaks were included for subsequent SA/CGM refinement of the above structures. Only low-velocity SA/CGM was performed at this stage, since the conformational changes needed to satisfy the additional restraints were small. Using this approach, the above structures were further refined to give 40 initial structures with an average total penalty of 0.024 ± 0.002 $Å^2$ (maximum total penalty = 0.032 $Å^2$) (Table 1). Superposition of backbone C, Cα, and N atoms of residues A1–L51 afforded an average pairwise root mean square (rms) deviation value of 0.57 ± 0.13 $Å^2$ (Table 1). A stereo drawing of the backbone atoms of residues A1–L51, obtained by superposition of the backbone atoms of residues A1–E14 and T27–L51, is shown in Figure 2.

Inspection of the above initial models enabled identification of several potential hydrogen-bonded groups. For example, despite the apparent scatter in Figure 2 for residues A15–G26, the folding of several residues within this region is consistent with the presence of classical tight turns. Specifically, residues D13–G17, D18–G22, and S24–T27 are folded to form two 3_{10}-helical corners and a Type-II β-turn, respectively. In addition, residues K28–L32, P33–W36, and P44–F48 are folded to form a 3_{10}-helical corner, a Type-I β-turn, and a 3_{10}-helical corner, respectively. The backbone amide protons of D18 and I23 are positioned to allow hydrogen bonding to the backbone carbonyls of I23 and D18, respectively, forming a non-idealized mini-β-sheet.

Although the relative orientations of the hydrogen-bonded atoms within all of the DG structures were consistent with the above hydrogen bonds, the observed NH–O distances exceeded the distances expected for ideal NH–O hydrogen bonds in several of the structures. In order to ensure that all of the inferred hydrogen bonds contain reasonable donor-acceptor distances, additional hydrogen bond restraints were included for subsequent refinement. It should be noted that it was not possible to determine the relative magnitudes of NH exchange rates for all of these protons due to signal overlap. In addition, one of the proposed hydrogen bonds involved the E14 NH proton, and this proton clearly exchanges with solvent deuterium within 20 min of incubation in D_2O (Fig. 1). However, the 2D NOESY cross peak patterns and the relative orientations of appropriate atoms in all of the DG structures are consistent with the presence of this and the other hydrogen bond-stabilized turns. As described below, final DG/SA structures were ultimately generated by addition of new restraints to limit the maximum separation of these NH–O atom pairs to 2.2 Å. This led to some improvement in the degree of convergence observed for the tight turns (see below), but did not alter the relative orientations observed in the initial models.

Additional hydrogen-bonded groups were identified from inspection of the initial models. First, the side chain amide group of Asn 21 is explicitly oriented in the direction of Asp 20 and/or Asp 18 (due to stereospecific NOE restraints for the Asn 21 side chain β and amide protons and the presence of several inter- and intraresidue NOEs). In addition, the Asn 21 NH^e side chain proton exhibits an unusually large downfield NMR chemical shift (9.5 ppm; compared to the random coil shift of ca. 7.5 ppm [Wüthrich, 1986]), suggesting its involvement in a hydrogen bond. Unfortunately, chemical shift degeneracy observed for the Asp 20 β-methylene protons precluded their stereospecific assignment, and in the initial models, the Asp 20 side chain group was moderately disordered. However, the Asp 18 carboxyl group in these models was directed toward the Asn 21 residue. Although either of these Lewis base groups could form a hydrogen bond with the Asn 21 NH^e proton, we tentatively assigned the hydrogen bond to the Asp 20 side chain carboxyl. Limited NOE data consistent with this assignment included (1) the presence of a very weak Asn-NH-to-Asn-NH^e NOE cross peak (which was expected to be stronger if the NH^e proton was directed toward Asp 18), (2) the lack of a strong Asn-NH^e-to-Asp 18-Hβ,β' cross peak, which would also be expected if Asn–Asp 18 hydrogen bonding were present. The usefulness of this NOE information was limited due to the moderately rapid exchange among the Asn-$NH^{e,z}$ protons and with solvent protons. However, electron density in the X-ray data (Day et al., 1992) show clearly that the actual hydrogen bond acceptor is Asp 18 (see companion paper [Blake et al., 1992a] and Kinemage 4).

Other hydrogen bonds were implicated on the basis of relative side chain orientations. Specifically, the side chain carboxyl of Asp 13 is oriented in a manner consistent with

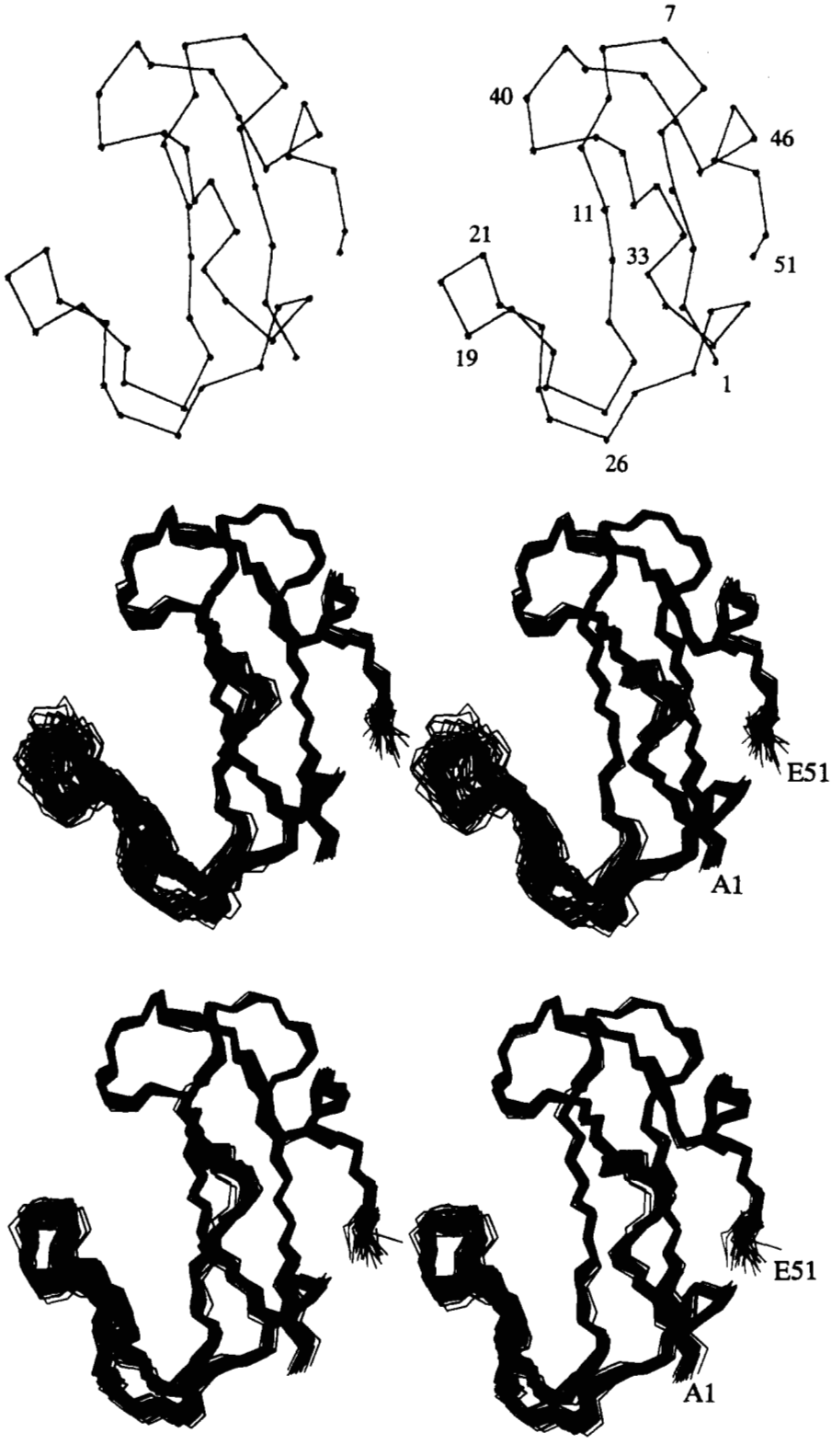

Fig. 2. Stereo views showing the superposition of the backbone atoms (C, Cα, N) of residues A1–E14 and T27–L51 for the 40 initial (middle) and final (bottom) distance geometry/simulated annealing (DG/SA) structures. Disordered residues E52 and D53 are not shown (see Fig. 3). These drawings illustrate the improved convergence that was achieved for residues A16–G26 (loop structure at the lower left side of the molecule) when hydrogen bond restraints for the helical corners and β-turns were included during refinement (see text for details). A mean Cα trace, with residues labeled, for the 40 final DG/SA structures is included at the top of the figure.

hydrogen bonding to the Asp 15 backbone amide, forming an Asx-type turn (Richardson, 1981; Rees et al., 1983; Abbadi et al., 1991). The carboxyl group of Asp 18 is oriented in a manner consistent with hydrogen bonding to the Trp 36 side chain amide proton. The Glu 14 side chain carboxyl is also poised to serve as a hydrogen bond acceptor for the Trp 3 side chain proton (Kinemage 3). Although signal overlap precluded measurement of the W3-NH^{ε} exchange rate, NOE cross relaxation between the NH^{ε} and H^{2} protons of W3 and the γH protons of

E14 provides experimental support for the W3-NH$^{\varepsilon}$ to E14-O$^{\varepsilon}$ hydrogen bond. Although the amide exchange rate of F29 is relatively fast (this proton exchanges completely with deuterium within 20 min of incubation in D_2O at 25 °C), this NH proton is also oriented (via NOE restraints) to form a hydrogen bond with the side chain carboxyl group of E14. NOEs also imply hydrogen bonding between the T27-OH proton and the S24-backbone carbonyl. It is important to note that the additional hydrogen bond restraints that were included for generation of the final structures were only added in order to ensure that the donor–acceptor distances were reasonable for all of the DG structures. These additional restraints did not alter the relative orientations of the hydrogen bond donor–acceptor groups. A complete list of the hydrogen-bonded atom pairs implicated by the NMR and structural information is included in Table 3.

The above 40 initial DG/SA structures were further refined using additional hydrogen bond restraints described above (except for the E14–W3 hydrogen bond), affording 40 final structures with penalties of 0.024 ± 0.003 Å^2 and with a maximum total penalty of 0.035 Å^2 (Table 1). These structures are superposed in the bottom of Figures 2 and 3 (see also Kinemage 1). For best visual comparison with the initial structures, only the backbone atoms of residues A1–E14 and T27–L51 are superposed in Figure 2. From this figure it is apparent that the addition of hydrogen bond restraints for the helical corners and β-turns led to improved convergence in these regions of the protein model. However, these restraints did not influence the global protein folding or the high convergence of the β-sheet and metal center that was observed in the initial structures. The backbone C, Cα, and N atoms of residues A1–L51 converged to give pairwise rms deviations of 0.42 ± 0.07 Å (Table 1). Superposition of all heavy atoms for residues A1–L51 and A1–D53, including conformationally nonrestricted groups, afforded pairwise rms deviation values of 0.72 ± 0.08 Å and 1.08 ± 0.22 Å, respectively (Table 1). Superposition of the backbone atoms of the final structures relative to the mean backbone coordinates (residues A1–L51) afforded pairwise rms deviation values of 0.29 ± 0.07 Å. Additional statistical information regarding the mean atom positions are given in Table 2.

The scatter observed for the C-terminal E52 and D53 residues probably accurately reflects conformational disorder in solution (Fig. 3). Thus, the backbone amide proton of residue E53 exhibited moderately intense NOE cross peaks to all of the side chain protons of residue D52. In addition, the D52 amide exhibited moderately intense NOE cross peaks to both the backbone NH and αH protons of the preceding L51 residue, consistent with the presence of a rapid conformational equilibrium on the NMR time scale (> ca. 50 ms).

On the other hand, we do not have direct evidence regarding the conformational mobility of other regions of the protein that exhibit a lower degree of convergence. Specifically, small disorder for the Type-I β-turn involving residues P33–W36 may result, in part, from the fact that our primary restraints for the proline five-membered rings may not be optimal. Thus, with the normal DSPACE primary restraints, small changes in internal proline torsion angles do not lead to significant penalty changes. This is an inherent problem encountered with five-membered rings, where the van der Waals contributions between all heteroatom pairs within five-membered rings are neglected. To maintain some degree of internal conformational rigidity, two nonbonded internal distance restraints were added that restrict the separation of the ProCδ to ($n-1$)Cα and ProCβ to ($n-1$)C atom pairs. In the future, we hope to generate a better set of primary distance restraints for proline residues that more accurately reflects internal conformations observed in protein crystal structures. In addition, fewer NOE cross peaks were observed for the backbone amide protons of residues D34 and D35,

Table 3. *Hydrogen bonds in Pyrococcus furiosus zinc-substituted rubredoxin*

β-sheet		Others	
o[1]	hn[14]	hn[16]	o[13]
o[2]	hn[51]	hn[17]	o[13]/o[14][a,b]
hn[3]	o[12]	hn[21]	o[18]
o[3]	hn[12]	hn[22]	o[19]
hn[4]	o[49]	hn[31]	o[28]
o[4]	hn[49]	hn[32]	o[29]
hn[5]	o[10]	hn[47]	o[44]
hn[6]	o[47]	hn[48]	o[45]
hn[18]	o[23][c]	hn[26]	o[14][b]
o[18]	hn[23][c]		
		hn[27]	o[24]
o[36]	hn[45]	hn[36]	o[33]
hn[38]	o[43]		
Metal site		Involving side chains	
o[5]	hn[9]	he1[3]	oe1[14][b]
hn[7]	sg[5]	hn[15]	od1[13]
hn[8]	sg[5]	hn[29][d]	oe1[14][b]
hn[10]	sg[8]		
o[38]	hn[42]	hh[12][d]	o[27][b]
hn[40]	sg[38]	hd2e[21][d]	od1[18][e]
hn[41]	sg[38]	hg1[27][d]	o[24]
hn[43]	sg[41]	he1[36]	od1[18]

[a] Based on the scatter in the orientations of the distance geometry (DG) structures, hydrogen bonding could occur to either of these oxygen atoms.

[b] No implicit hydrogen bond restraints were included for these atom pairs during DG structure refinement.

[c] These were the only two β-sheet hydrogen bonds that were not included as restraints during the generation of the initial DG/SA structures.

[d] The proton exchange rates exceed 0.1 min^{-1} at 25 °C. Complete exchange with solvent (D_2O) within 20 min at 25 °C.

[e] The hydrogen bond acceptor was tentatively assigned as od1[20], based on limited nuclear Overhauser effect data. X-ray diffraction results clearly identified the acceptor as od1[18] (see text).

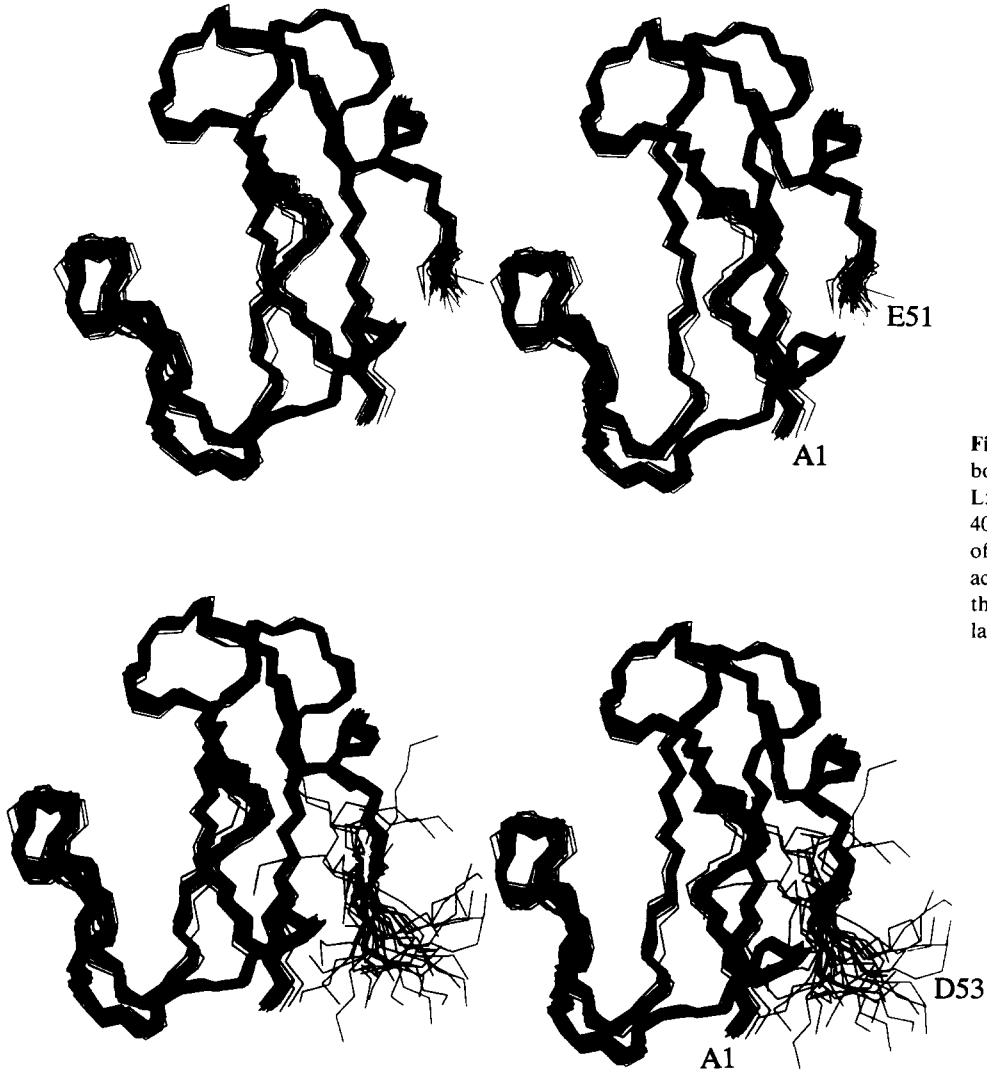

Fig. 3. Stereo views showing the backbone atoms (C, Cα, N) of residues A1–L51 (top) and A1–D53 (bottom) of the 40 final DG/SA structures. The scatter of the C-terminal E52 and D53 residues accurately reflects the NMR observation that these residues are conformationally labile (see text).

and this reduction in distance information probably also contributed to the relatively poorer convergence of this Type-I β-turn.

Other regions of the protein also exhibit a small amount of conformational disorder. For example, residues D15–G26 are structurally self-consistent (pairwise rms deviation values for C, Cα, and N backbone atoms of these residues = 0.35 ± 0.11 Å); however, their positions relative to the rest of the protein are not as precisely defined (see Fig. 2). It is possible that the disorder reflects the fact that fewer long-range NOE restraints from this loop to the rest of the protein were available from the NMR data.

Structure evaluation on the basis of 2D NOESY back calculations

The final DG structures were evaluated in terms of consistence with experimental NMR data by performing 2D NOESY back calculations on a representative low-penalty structure. Generic cross relaxation and z-leakage rate constants of −0.23 and 0.93 s^{-1} were determined as described (Summers et al., 1991) and were used as input for the program BKCALC®. The BKCALC algorithm calculates the time course of each proton by numeric integration of the Bloch equations in a manner that quantitatively accounts for spin diffusion effects (Summers et al., 1990). The downfield regions of the experimental and back-calculated 200-ms NOESY spectra are compared in Figure 4. Although a quantitative comparison of relative cross peak intensities has not been performed, visual inspection reveals that the experimental and back-calculated spectra are qualitatively similar in appearance. In particular, the back-calculated sequential NH-NH and NH-αH cross peak patterns and their relative intensities match the experimental data (Fig. 4), and this indicates that the backbone folding of the DG/SA structures is consistent with the solution-state protein conformation. Cross peak patterns involving many side chain protons are also generally in good agreement; e.g., see cross peaks involving aromatic protons in Figure 4. Although all protons were

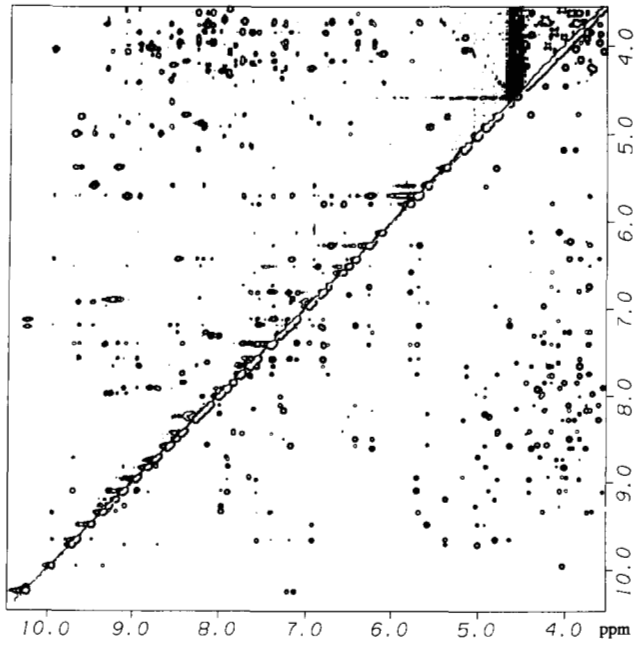

Fig. 4. Downfield portions of the experimental (above diagonal) and back-calculated (below diagonal) two-dimensional nuclear Overhauser effect (NOESY) spectra for *P. furiosus* Zn(Rd). The experimental data were collected with a mixing time of 200 ms at 45 °C. The simulated 200-ms NOESY spectrum was back-calculated with single cross relation and z-leakage rate constants of -0.23 and $0.93\ s^{-1}$, respectively. Differential z-leakage rates due to chemical exchange with presaturated solvent protons have not been included in the calculations. The similarity of relative intensities of sequential NH(i)-NH($i-1$) and NH(i)-αH($i-1$) and long-range Hα-Hα, NH-aromatic, Hα-aromatic, and aromatic-aromatic cross peaks indicates that the backbone and global folding of the distance geometry structure is consistent with the experimental data.

included in the NOESY time course calculations, only the protons of the conformationally restricted groups were considered when evaluating the consistence between the experimental and back-calculated spectra.

The current NOESY back calculations did not account for the reduced intensities of several labile amide and OH protons that result from chemical exchange with presaturated water protons, or for the larger z-leakage rates associated with these protons. In addition, the reduced intensities of several αH protons with frequencies close to or at the water frequency were also not accounted for in the calculations. For these reasons, a quantitative comparison of the experimental and back-calculated NOESY data, which ultimately may provide an R-value similar to those used to define certainties in X-ray structures, was not performed. It should be noted that, unlike for X-ray crystallographic measurements, signals for groups that are in rapid conformational equilibria often give rise to the most intense NOE cross peaks (due to differences in local correlation times). For this reason, we believe that it will be impractical to determine an R-value for the entire set of NOESY data, and that discretion must ultimately play a role in determining which NOESY cross peaks can realistically be modeled using a single correlation time/static model approach.

However, even when used only for qualitative comparisons, NOESY back calculations can greatly facilitate structure refinement by identifying the experimentally most-consistent single structure among many substructures generated during the refinement process. This situation arises most often when structures are generated using only a limited number of restraints for a particular protein segment. For example, in studies of a zinc-containing metallopeptide (South et al., 1991), overlap of two NH proton signals of sequential residues confounded assignment of the NOE cross peaks associated with these protons. No distance restraints were employed for these protons, and as a consequence, the initial DG structures contained two different backbone amide orientations for these residues (involving a 180° flip of a single peptide linkage). In that case, NOESY back calculations enabled identification of the single orientation consistent with the experimental NOESY spectra (South et al., 1991). In the present study, however, the DG/SA structures converged to a single backbone conformation due to the application of a large number of distance restraints for each residue. Thus, for the present study, back calculations were not essential to the structure refinement process, although they greatly facilitated the final evaluation of the structures in terms of their consistence with the experimental NOESY data.

Description of the folding and comparison with C. pasteurianum Rd

As predicted from secondary structural NMR studies, residues A1–C5, Y10–E14, and F48–L51 of *P. furiosus* Zn(Rd) form a three-stranded antiparallel β-sheet (see Figs. 2, 3; Kinemage 1). Two additional short stretches of antiparallel β-sheet-like structure involving residues G17–P19 paired with I23–S24 and residues W36–C38 paired with P44–K45 are also apparent. Residues C5–Y10 and C38–A43 form a series of Types-I, -II, and -III NH–S tight turns, and residues D13–G17, D18–G22, K28–L32, and P44–F48 are folded to form four 3_{10}-helical corners. In addition, the side chain of D13 appears to be hydrogen bonded to the amide of D15, forming an Asx turn (Richardson, 1981; Rees et al., 1983; Abbadi et al., 1991), and residues P25–T27 and P33–W36 form Types-I and -II β-turns, respectively. The hydrophobic side chains of residues W3, Y10, Y12, I23, F29, L32, W36, and F48 contribute to the hydrophobic core of the protein, with apparent stacking of the six-membered aromatic rings of Trp 3 and Phe 29 (Fig. 5; Kinemage 2).

The above structural elements are surprisingly similar to those observed in the high-resolution X-ray structure of native *C. pasteurianum* Rd. As shown in Figure 6, the average psi and phi values for the final DG/SA structures

Fig. 5. Stereo view showing the hydrophobic core for the 40 final DG/SA structures. Backbone C, Cα, and N atoms of residues A1–L51 were superposed (root mean square [rms] deviation = 0.42 ± 0.07 Å); for clarity, only the backbone atoms of one representative final DG/SA structure are displayed. All of the side chain heteroatoms of residues that comprise the hydrophobic core of the protein, including W3, Y10, Y12, I23, I32, W36, and F48, are displayed.

of *P. furiosus* Zn(Rd) compare favorably with those of *C. pasteurianum* Rd (see also Supplementary Figure S1, Diskette Appendix). Superposition of the backbone C, Cα, and N atoms of residues A1–L51 of *P. furiosus* Zn(Rd) onto relevant atoms of residues K2–V52 of *C. pasteurianum* Rd affords an average pairwise rms deviation of 0.77 ± 0.06 Å (Table 1; Fig. 7; Kinemage 1). Thus, the enhanced thermal stability of *P. furiosus* Rd relative to *C. pasteurianum* Rd is not due to differences in global tertiary structure.

It is noteworthy that the metal-binding sites of *P. furiosus* Zn(Rd) and native *C. pasteurianum* Rd also appear to have similar conformations. Superposition of the C, Cα, N, Cβ, and Sγ atoms of the metal coordination site residues C5–Y10 and C38–A43 of *P. furiosus* Zn(Rd) onto relevant residues C6–Y11 and C39–V44 of native *C. pasteurianum* Rd afforded pairwise rms deviation values of 0.33 ± 0.02 Å. These structural findings lend further sup-

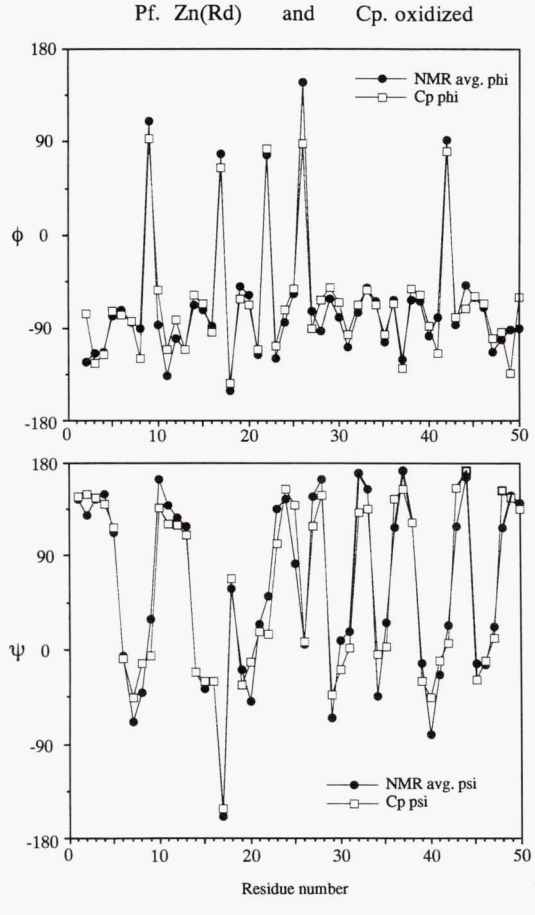

Fig. 6. Plots of the average phi (top) and psi (bottom) values for the 40 final DG/SA structures of *P. furiosus* Zn(Rd). The average standard deviation in phi and psi is ca. ±11°, with variations generally paralleling deviations in Cα position (Fig. 10). For comparison, relevant values obtained from the X-ray structure of *Clostridium pasteurianum* oxidized rubredoxin (Cp) (Watenpaugh et al., 1979) are also presented.

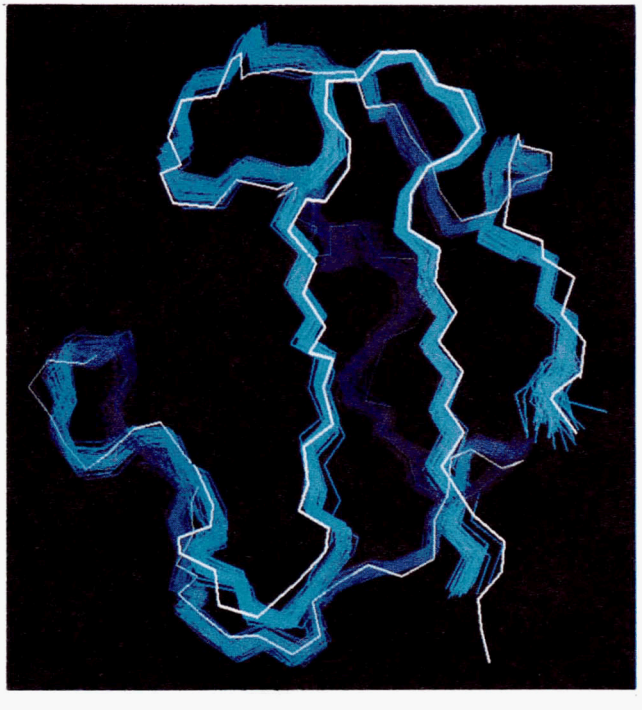

Fig. 7. Superposition of the backbone C, Cα, and N atoms of residues A1–L51 of *P. furiosus* Zn(Rd) (blue) with appropriate backbone atoms of *C. pasteurianum* Rd (white) (pairwise rms deviation = 0.77 ± 0.06 Å), showing the similarity of the global protein folding.

port for the use of zinc in NMR studies of paramagnetic metalloproteins since this substitution has not caused a significant structural perturbation at the metal-binding site.

Several hydrogen bonds involving side chain groups that were observed in the X-ray structure of *C. pasteurianum* Rd have also been observed in *P. furiosus* Zn(Rd). The NH^{ε} proton of W36 is in slow chemical exchange with solvent protons, suggesting that this proton may be involved in a hydrogen bond. In addition, several NOE cross peaks involving the Hβ protons of D18 implicitly direct the side chain carboxyl group of D18 toward the center of the protein and in the direction of the W36-NH^{ε} proton. Many of the initial DG structures generated without side chain hydrogen bond restraints exhibited W36-NH^{ε}-to-D18-O^{δ} distances consistent with such hydrogen bonding (corresponding to residues W36 and D19 in *C. pasteurianum* Rd). The final structures also reflect the extensive NOE data associated with the hydroxyl protons of Y12 and T27, which positions these protons in close proximity to (and are apparently hydrogen bonded with) the backbone carbonyls of residues T27 and S24, respectively (Table 3). Several additional hydrogen bonds that are unique to *P. furiosus* Rd are discussed below.

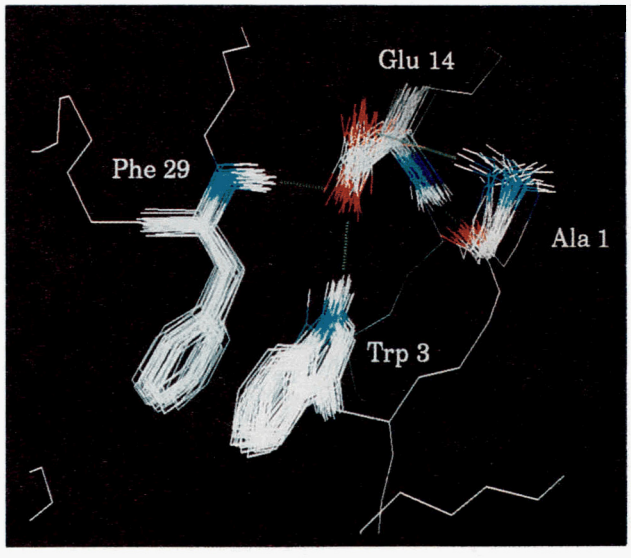

Fig. 8. Figure showing the important hydrogen bonding and electrostatic interactions that are believed to be responsible for the stabilization of the N-terminal end of the three-stranded β-sheet. Displayed in the figure are the nonconserved (compared to other rubredoxins) Trp 3 and Glu 14 residues, along with Phe 29 and the N-terminal NH_3^+ of Ala 1. The figure was generated by superposing the backbone C, Cα, and N atoms of residues A1–L51 only. Dotted green lines represent hydrogen bonding or potential electrostatic interactions.

Determinants of protein hyperthermostability

Despite the high similarity of the globular folding observed for *C. pasteurianum* and *P. furiosus* rubredoxins, several key structural differences exist. These differences provide insights into what may be the molecular-level determinants of hyperthermostability in *P. furiosus* Rd. First, as indicated from preliminary analysis of NOE cross peak patterns (Blake et al., 1991b), the β-sheet of *P. furiosus* Zn(Rd) extends to the N-terminal Ala, providing an additional hydrogen bond that apparently does not exist in the β-sheet of *C. pasteurianum* Rd. In addition, the occurrence of a Glu residue at position 14, combined with the shortening of the protein by one residue at the N-terminal end, leads to apparent electrostatic stabilization of the N-terminal amino group, which is placed in close proximity to the carboxyl group of residue Glu 14. These structural elements were identified earlier on the basis of qualitative secondary structure analysis of 2D NOESY data (Blake et al., 1991a). In addition, the W3-NH^{ε} and F29-NH protons are positioned to hydrogen bond to the E14 side chain carboxyl oxygen atoms. Interestingly, *P. furiosus* Rd is the only known Rd with residues that are capable of forming such hydrogen bonds. These combined interactions appear to confer structural stability to the N-terminal end of the three-stranded β-sheet (see Figs. 8, 9; Kinemage 3).

Interestingly, large temperature factors were obtained for the two N-terminal residues of *C. pasteurianum* Rd (Fig. 10), indicating that these residues are relatively disordered in the crystal form of the protein. In contrast, the N-terminal Ala 1 of *P. furiosus* Rd exists in a unique conformation (Figs. 8–10). It thus appears that the N-terminal end of *P. furiosus* is *less labile* than that of *C. pasteurianum* Rd, and this finding is consistent with our hypothesis that hyperthermostability may reflect a decreased tendency for the N-terminal end to "unzip" at elevated temperatures (Blake et al., 1991b).

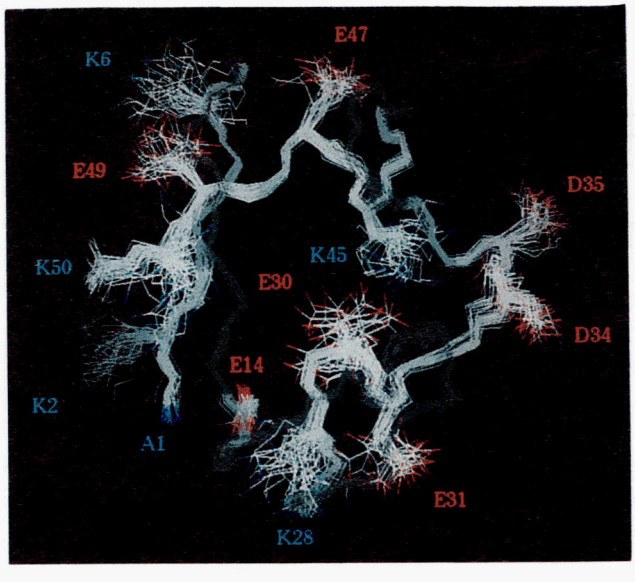

Fig. 9. Superposition of DG/SA structures (backbone atoms; see Fig. 8) of *P. furiosus* Zn(Rd) showing the relative locations of all of the basic and most of the acidic surface residues.

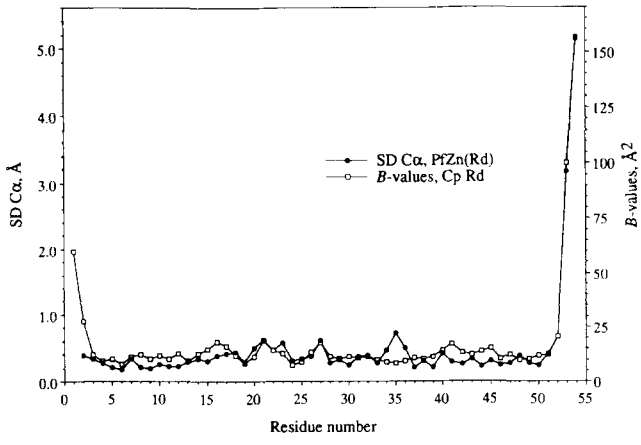

Fig. 10. Comparison between the crystallographic *B*-values of the Cα carbons of *C. pasteurianum* Rd with the standard deviation from the mean Cα coordinates of the 40 final DG/SA structures of *P. furiosus* Zn(Rd). Relatively large *B*-values associated with residues Met 1 and Lys 2 are indicative of conformational disorder in *C. pasteurianum* Rd. In contrast, the standard deviation observed for the N-terminal Ala 1 (aligned with Lys 2 in this figure) of *P. furiosus* Rd is small, reflecting conformational stability.

Other structural elements may also contribute to protein hyperthermostability. *Pyrococcus furiosus* Zn(Rd) contains a hydrogen bond between the side chain NH proton of N21 and the side chain carboxyl group of D18 (Kinemage 4). Similar hydrogen bonding was not present in *C. pasteurianum* Rd, which contains two Asp residues at the relevant positions. This hydrogen bond may lend additional stability to the associated D18–G22 helical corner. In addition, the side chain amino groups of K45 and K28 are positioned in close proximity to the side chain carboxyl groups of E30 (and/or D34) and E31, respectively. *Pyrococcus furiosus* Rd is also the only known Rd that contains a basic amino acid within the metal-binding loops (K6), and K6-$NH3^+$ to E49 (and/or E47)-COO^- electrostatic interactions may provide additional stabilization to this region of the protein (Fig. 9). The precise assignment of unique side chain conformations of these residues (if a unique conformation indeed exists in solution) could not be made with the present data and will only be possible using higher dimensional heteronuclear-edited NMR methods and isotopically labeled protein samples.

Summary

Because the backbone folding of *P. furiosus* Zn(Rd) is essentially identical to that of *C. pasteurianum* Rd, the enhanced thermal stability of *P. furiosus* Rd cannot be attributed to differences in global protein structure. There are, however, structural and apparent dynamic differences among the N-terminal residues of the two proteins. In particular, relatively large thermal parameters are associated with the Cα atoms of residues Met 1 and Lys 2 of *C. pasteurianum* Rd (Fig. 10), reflecting either greater thermal motion or disorder. These residues are not hydrogen bonded to other residues in the protein and are not incorporated into the three-stranded β-sheet. On the other hand, the N-terminal Ala 1 of *P. furiosus* Rd is structurally well defined, and NOE cross peak patterns indicate that this residue is incorporated into the three-stranded β-sheet hydrogen-bonding network. Thus, the enhanced thermal stability of *P. furiosus* Rd may result from a reduction in the lability of the N-terminal residues. This explanation is consistent with our proposal that the additional hydrogen bonding and electrostatic interactions inhibit the N-terminal end of the β-sheet from "unzipping" at elevated temperatures (Blake et al., 1991b).

It appears that four significant differences in amino acid sequence may be primarily responsible for the added interactions and associated stability of the N-terminal residues. First, *P. furiosus* Rd is shorter by one residue (a conserved Met) at the N-terminus compared to rubredoxins from mesophiles. Second, *P. furious* Rd is the only Rd to contain an Ala at position 1 (corresponding to position 2 of the rubredoxins from mesophiles), and the observed folding may explicitly require a nonbulky residue at this position in order to satisfy steric requirements. Third, *P. furiosus* Rd contains a Glu at position 14; the analogous position is normally occupied by Pro in mesophilic rubredoxins. The consequence of these changes is that the E14-COO^- group is juxtapositioned to interact with the N-terminal ammonium group of Ala 1 and the backbone amide proton of Phe 29. Fourth, the placement of a Trp at position 3 (found only in one other rubredoxin, which, interestingly, derives from the moderate thermophile *Clostridium thermosaccharolyticum*) allows an additional side chain–side chain hydrogen bond to occur between the $W3NH^e$ proton and the $E14CO^e$ carboxyl oxygen.

Other factors, such as the efficiency of hydrophobic packing in the protein core (e.g., see Lim & Sauer, 1991, and references therein), reverse hydrophobic effects of protein surface residues (Pakula & Sauer, 1990), or electrostatic stabilization due to the nonconservatively substituted Lys 6 within the metal-binding loop may also contribute to the enhanced thermal stability of *P. furiosus* Rd. NMR studies of the temperature-dependent structural and dynamic properties of *P. furiosus* Rd are now underway. We plan to carry out similar studies of *C. pasteurianum* Rd to test our hypothesis that protein denaturation may be initiated at the N-terminus of the β-sheet. In addition, studies of site-directed mutants of rubredoxins are now underway to investigate the relative contributions of individual amino acid residues on the global protein structure and thermal stability.

Materials and methods

Sample preparation

Zinc-substituted *P. furiosus* Rd was prepared as described previously (Blake et al., 1991b). Two-dimensional NMR

data for structural studies were obtained with a sample containing 7 mM Zn(Rd), 200 mM NaCl, and 25 mM acetate-d3 in 90% H_2O/10% D_2O at pH 6.3; $T = 45$ °C. Deuterium exchange experiments were performed with a sample containing 1.3 mM Zn(Rd) and solution conditions as described above (except as noted in the text).

NMR data collection and processing

Two-dimensional NMR data for structure determination were collected and processed as described previously (Blake et al., 1991b). The 600-MHz 2D NOESY (Jeener et al., 1979; Macura & Ernst, 1980) data were obtained in a GE Omega PSG-600 instrument with mixing times of 10, 50, 100, 200, 300, and 450 ms; $T = 45$ °C. The predelay period was adjusted for each experiment so that the total recycle time remained constant (3 s; = ca. 3 times the longest T_1). The 2D ROESY (Bothner-by et al., 1984) spectrum was obtained with an 80-ms, 6.1-kHz continuous wave spin lock field. Data were processed with 4.5-Hz Gaussian line broadening in t_1 and a 90° shifted-sine squared function in t_1 using FTNMR® and FELIX® software (Hare Research, Inc.). Cross peak and diagonal peak volumes used for NOESY back calculations were determined by volume integration with FTNMR.

Distance restraints

Primary distance restraints employed in these calculations, including nonbonded distances to enforce planarity of peptide bonds, have been published previously (Blake et al., 1991a). Atomic radii were also assigned previously published values, except that hydrogen atoms were assigned a radius of 0.8 Å. Zinc–sulfur distances were restrained to 2.3 Å, and additional nonbonded zinc–Cβ(Cys) restraints of 3.36 Å were included to enforce proper sp^3 hybridization of the Cys sulfurs. To allow for potential hydrogen-bonding interactions, the van der Waals radii of all atom pairs involving amide or hydroxyl protons and oxygen or sulfur atoms were reduced to allow these atoms to approach each other to distances equal to 75% (involving oxygen) or 90% (involving sulfur) of the sum of their normal van der Waals radii.

NOE-derived interproton distances were assigned boundary values of 1.8–2.7 Å, 1.8–3.3 Å, and 1.8–5.0 Å to represent strong, medium, and weak NOE cross peaks, respectively (Gronenborn et al., 1991), that were observed in a 200-ms 2D NOESY spectrum. An additional 0.5 Å was added to the upper bound for proton pairs that involved a methyl group (Clore et al., 1987).

Structure calculation and refinement

DG structures were generated and refined using an automated approach (Blake et al., 1991a) that included variable-velocity SA, differential weighting of the primary and NOE-derived distance restraints, and 4D SA/CGM refinement (Blake et al., 1991a). During the final stages of refinement, primary and NOE-derived distance restraints are given equal weighting. The structures were not subjected to more sophisticated energy minimization-type refinement. Structures were calculated with DSPACE using macros to automatically perform atom randomizations, SA, and CGM steps; these macros have been included in the supplementary material on the Diskette Appendix.

NOE back calculations

Two-dimensional NOESY back calculations were performed by numeric integration of the Bloch equations as described (Summers et al., 1990). A generic z-leakage rate constant (which accounts for loss of magnetization due to processes other than cross relaxation) of 0.92 s^{-1} was determined by plotting the natural log of the total integration of each 2D NOESY spectrum versus the mixing time. The cross relaxation rate constant was determined by visual best-fitting of the NOE time course data observed for several sequential αH-NH proton pairs of the β-sheet. We found this preferable to fitting fixed distances of other protons, such as those that occupy adjacent positions on aromatic rings or Hα-protons of glycines, due to the fact that these protons exhibit mutual scalar coupling which leads to significant zero-quantum artifact contributions to NOESY data obtained with mixing times of 200 ms or less.

Acknowledgments

Acknowledgment is made to the donors of the Petroleum Research Fund, administered by the American Chemical Society, for support of this work. This work was also supported by a National Science Foundation Research Training Group Award to the Center for Metalloenzyme Studies of the University of Georgia (DIR 9014281), and by grants to M.W.W.A. from the Office of Naval Research (N00014-90-J-1894) and the National Science Foundation (BCS-9011583). The 600-MHz NMR instrument at the University of Maryland Baltimore County (UMBC) was purchased with support from the NIH (grants GM42561 and AI30917 to M.F.S.). We gratefully acknowledge the assistance of Bernard J. Duffy (UMBC Academic Computing) for providing us with several custom programs for manipulating the protein coordinate files and for performing statistical analyses.

References

Abbadi, A., Mcharfi, M., Aubry, A., Prenilat, S., Boussard, G., & Marraud, M. (1991). Involvement of side functions in peptides structures: The Asx turn. Occurrence and conformational aspects. *J. Am. Chem. Soc. 113*, 2729–2735.

Adams, M.W.W. (1990). The metabolism of hydrogen by extremely thermophilic sulfur-dependent bacteria. *FEMS Microbiol. Rev. 75*, 219.

Baker, E.N. & Hubbard, R.E. (1984). Hydrogen bonding in globular proteins. *Prog. Biophys. Mol. Biol. 44*, 97–179.

Blake, P.R., Day, M.W., Hsu, B.T., Joshua-Tor, L., Park, J.-B., Hare, D.R., Adams, M.W.W., Rees, D.C., & Summers, M.F. (1992a). Com-

parison of the X-ray structure of native rubredoxin from *Pyrococcus furiosus* with the NMR structure of the zinc-substituted protein. *Protein Sci. 1*, 1522–1525.

Blake, P.R., Hare, D.R., & Summers, M.F. (1991a). Is 2-D NOESY back-calculation necessary for NMR-based structure determination1 A systematic study involving a retroviral-type zinc finger peptide. *Techniques Protein Chem. II*, 357–370.

Blake, P.R., Lee, B., Summers, M.F., Adams, M.W.W., Park, J.-B., Zhou, H.Z., & Bax, A. (1992b). Quantitative measurement of small through-hydrogen-bond and 'through space' 1H-113Cd and 1H-199Hg J couplings in metal-substituted rubredoxin from *Pyrococcus furiosus. J. Biomol. NMR 2*, 527–533.

Blake, P.R., Park, J.-B., Adams, M.W.W., & Summers, M.F. (1992c). Novel observation of NH–S(Cys) hydrogen bond-mediated scalar coupling in 113Cd-substituted rubredoxin from *Pyrococcus furiosus. J. Am. Chem. Soc. 114*, 4931–4933.

Blake, P.R., Park, J.-B., Bryant, F.O., Aono, S., Magnuson, J.K., Eccleston, E., Howard, J.B., Summers, M.F., & Adams, M.W.W. (1991b). Determinants of protein hyperthermostability: Purification and amino sequence of rubredoxin from the hyperthermophilic archaebacterium *Pyrococcus furiosus* and secondary structure of the zinc adduct by NMR. *Biochemistry 30*, 10885–10895.

Bothner-by, A., Stephens, R.L., Lee, J.T., Warren, C.D., & Jeanloz, R.W. (1984). Structure determination of a tetrasaccharide: Transient nuclear Overhauser effects in the rotating frame. *J. Am. Chem. Soc. 106*, 811–813.

Clore, G.M., Gronenborn, A.M., Nilges, M., & Ryan, C.A. (1987). Three-dimensional structure of potato carboxypeptidase inhibitor in solution. A study using nuclear magnetic resonance, distance geometry, and restrained molecular dynamics. *Biochemistry 26*, 8012–8023.

Day, M.W., Hsu, B.T., Joshua-Tor, L., Park, J.-B., Zhou, Z.H., Adams, M.W.W., & Rees, D.C. (1992). X-ray crystal structures of the oxidized and reduced forms of the rubredoxin from the marine hyperthermophilic archaebacterium *Pyrococcus furiosus. Protein Sci. 1*, 1494–1507.

Fiala, G. & Stetter, K.O. (1986). *Pyrococcus furiosus* represents a novel genus of marine heterotrophic archaebacteria growing optimally at 100 °C. *Arch. Microbiol. 145*, 56–61.

Gronenborn, A.M., Filpula, D.R., Essiz, M.Z., Achari, A., Whitlow, M., Wingfield, P.T., & Clore, G.M. (1991). A novel, highly stable form of the immunoglobulin binding domain of streptococcal protein G. *Science 253*, 657–661.

Jeener, B.H., Meier, P., Bachmann, P., & Ernst, R.R. (1979). Investigation of exchange processes by two-dimensional NMR spectroscopy. *J. Chem. Phys. 71*, 4546–4553.

Lim, W.A. & Sauer, R.T. (1991). The role of internal packing interactions in determining the structure and stability of a protein. *J. Mol. Biol. 219*, 359–376.

Macura, S. & Ernst, R.R. (1980). Elucidation of cross relaxation in liquids by two-dimensional N.M.R. spectroscopy. *Mol. Phys. 41*, 95–117.

Pakula, A.A. & Sauer, R.T. (1990). Reverse hydrophobic effects relieved by amino acid substitutions at a protein surface. *Nature 344*, 363–364.

Rees, D.C., Lewis, M., & Lipscomb, W.N. (1983). Refined crystal structure of carboxypeptidase A at 1.54 Å resolution. *J. Mol. Biol. 168*, 367–387.

Richardson, J.S. (1981). The anatomy and taxonomy of protein structure. *Adv. Protein Chem. 34*, 167–339.

South, T.L., Blake, P.R., Hare, D.R., & Summers, M.F. (1991). C-terminal retroviral-type zinc finger domain from the HIV-1 nucleocapsid protein is structurally similar to the N-terminal zinc finger domain. *Biochemistry 30*, 6342–6349.

Stetter, K.O. (1986). Diversity of extremely thermophilic archaebacteria. In *The Thermophiles: General, Molecular and Applied Microbiology* (Brock, T.D., Ed.), pp. 39–74. John Wiley, New York.

Stetter, K.O., Fiala, G., Huber, G., Huber, R., & Segerer, G. (1990). Hyperthermophilic microorganisms. *FEMS Microbiol. Rev. 75*, 117–124.

Summers, M.F., South, T.L., Kim, B., & Hare, D.R. (1990). Structure of an HIV zinc fingerlike domain via a new NMR based distance geometry approach. *Biochemistry 29*, 329–340.

Watenpaugh, K.D., Sieker, L.C., Herriott, J.R., & Jensen, L.H. (1973). Refinement of the model of a protein: Rubredoxin at 1.5 Å resolution. *Acta Crystallogr. B29*, 943–956.

Watenpaugh, K.D., Sieker, L.C., & Jensen, L.H. (1979). The structure of rubredoxin at 1.2 Å resolution. *J. Mol. Biol. 131*, 509–522.